COBEM 2023 27TH INTERNATIONAL CONGRESS OF MECHANICAL ENGENEERING

ABCM Brazilian Society of Mechanical Sciences and Engineering
27th ABCM International Congress of Mechanical Engineering
December 04-08, 2023, Florianópolis-SC, Brazil

COB-2023-1991
INVESTIGATION OF THE EFFECTS OF STRUCTURAL NONLINEARITIES ON AEROELASTIC LCOS

Lucas Pereira Resende
Polliana Cândida Oliveira Martins
Brasília University (UnB) - Aeroespace Engineering - Campus Gama, Setor Leste Projeção A - Gama Leste, Brasília, DF, ZIP CODE 72444-240, fga.unb.br
lucasperesende@gmail.com
polliana.martins@unb.br

Abstract. *Aeroelasticity deals with the study of the interaction between aerodynamic forces and structural dynamics, being crucial for the safety, performance, and efficiency of aerospace vehicles. Some aeroelastic phenomena, if not adequately addressed, can cause structural deformations that may lead to structural failure or performance loss. In this context, the importance of considering nonlinear effects in the study of aeroelasticity has become more evident with the advancement of aerospace systems, which are increasingly lighter and have challenging geometries. Therefore, this study proposes the analysis of the effects of structural nonlinearities, such as cubic stiffness, in an aeroelastic model of a straight rectangular wing with three degrees of freedom (bending, torsion, and control surface torsion). The model was initially analyzed in the classical linear domain of frequency, using the eigenvalue solution to calculate the critical flutter speed, natural frequencies, and associated damping. Along with the straight wing model, an aerodynamic model using strip theory simplification was used. The critical speed was calculated and compared with results from the literature. Then, the analysis proceeded in the time domain, using the 4th order Range-Kutta integration method to integrate the equations of motion and visualize the oscillation amplitudes of the treated degrees of freedom. A nonlinear model in the time domain was constructed by introducing a structural nonlinearity (cubic stiffness) in the model's stiffness. The presence of nonlinearities in the stiffness of the three degrees of freedom was evaluated. Based on the analysis of the results, it was observed that by introducing cubic stiffness in the wing's torsional mode, there was an increase in damping at the critical velocity of the linear model. Various nonlinear coefficients were tested, and the responses were compared with the linear case to highlight the differences in the treated values and the importance of including nonlinear behavior to detect Limit Cycle Oscillations (LCOs) and critical behaviors.*

Keywords: *Aeroelasticity, nonlinear effects, stiffness, Flutter, Limit Cycle Oscillations*

1. INTRODUCTION

Since the early controlled flights in the 20th century, engineers and designers have grappled with challenges related to the interaction between aerodynamic forces and the structural flexibility of aircraft. It became evident that wing flexibility could lead to undesirable oscillations that could compromise aircraft stability and safety. The field of aeroelasticity, a branch of aeronautical science, deals precisely with the interactions between inertial, elastic, and aerodynamic forces [Bisplinghoff, Ashley, and Halfman, 1996].

The term "aeroelasticity" emerged a little over a century ago when pioneers like Roxbee Cox and Pugsley began correlating studies on aileron control, rolling capability, and investigations into flutter [Collar, 1946]. Aeroelasticity encompasses both static and dynamic phenomena. Static phenomena, such as divergence and control reversal, arise when aerodynamic and elastic forces are analyzed together. Additionally, the distribution of loads is influenced by the structure's elasticity.

Dynamic aeroelastic phenomena, like buffeting, gust response, and flutter, arise when inertial, elastic, and aerodynamic forces interact simultaneously. Flutter, in particular, is a dynamic instability associated with the interaction of these forces and is one of the most significant issues in aeroelasticity [Hodges and Pierce, 2002]. Flutter involves self-sustained oscillations in the aircraft's structure when subjected to significant lateral aerodynamic loads, with catastrophic potential if not adequately controlled [Wright and Cooper, 2015].

The history of aviation records notable cases of flutter, such as the incident with the Handley-Page bomber and the resolution of flutter issues in the F-111C aircraft. These events helped establish the foundations for the study and understanding of aeroelastic phenomena, crucial for the design of safe and efficient aircraft.

In recent years, with technological advancements, it has become crucial to consider nonlinear effects in aeroelasticity. Nonlinear effects can arise in both aerodynamics, due to shocks and flow separation, and in the elastic structure, due to clearances, friction, and nonlinearities in structural stiffness [Sharma, 2005]. Nonlinear aeroelasticity focuses on under-

standing nonlinear interactions and phenomena such as Limit Cycle Oscillations (LCO), which are damped oscillations of the structure and represent variations of flutter with limited amplitudes.

This study aims to address the challenge of understanding the implications of nonlinearities in aeroelastic systems by developing an analytical model that takes these nonlinear characteristics into account, thereby contributing to the improved understanding and prediction of complex behaviors in aeroelasticity.

2. ANALYTIC MODEL

2.1 Aeroelastic equation of motion for three degrees of freedom

This paper employs a conventional bending/torsion aeroelastic model, incorporating a control surface connected to its end via a torsional spring deducted by Wright and Cooper (Wright and Cooper (2015)). In this model, downward heave (z) is considered positive, while clockwise rotation of both pitch (θ) and the control (β) are regarded as positive.

The translational deflection (z), positive downward, can be expressed as a combination of the generalized coordinates q_b, q_t, and β, the rotation of the control surface, as follows:

$$z = \left(\frac{y}{s}\right)^2 q_b + \left(\frac{y}{s}\right)(x - x_f)q_t + [x - x_h]\beta = \phi_b q_b + \phi_t q_t + \phi_\beta \beta \tag{1}$$

Based on the previously mentioned information and Equation 1, it can be affirmed that the addressed model can be mathematically described as a contribution of the assumed modes of bending, ϕ_b, torsion, ϕ_t, and control surface deflection, ϕ_β.

Figure 1 depicts the plate wing with a control surface attached, illustrating the chord (c) and wing span (s). Additionally, it highlights the positions of the hinge line (x_h), elastic line (x_f), and aerodynamic line (x_{ac}). The airflow is denoted by V, while k_α, k_h, and k_β represent the torsional, translational, and control surface rotational stiffness, respectively.

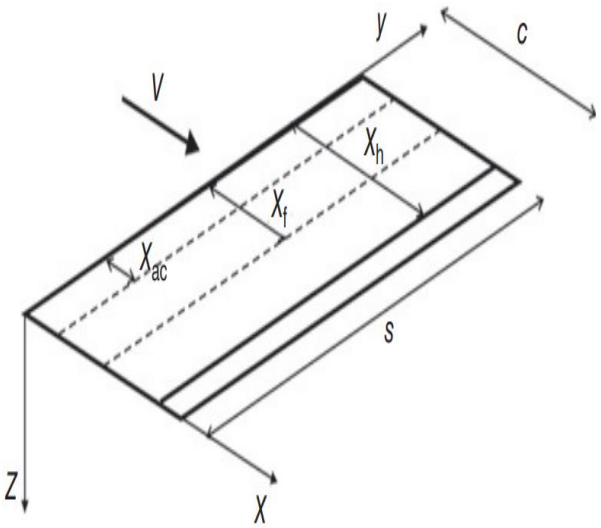

Figure 1. Three degree of freedom wing model Wright and Cooper (2015)

For the aerodynamic matrices, it is used the same approach as (Wright and Cooper (2015)), with the addition of considering the influence of the control surface rotation. To define the model, we chose to employ a simplified version of the unsteady aerodynamic model, which allows us to perform time integration.

Using the model derived by Wright and Cooper, it is obtained the aeroelastic equations for a straight rectangular wing with three degrees of freedom, involving the interaction between bending, torsion, and control surface rotation (Equation 2).

$$\begin{bmatrix} A_{bb} & A_{bt} & A_{b\beta} \\ A_{tb} & A_{tt} & A_{t\beta} \\ A_{\beta b} & A_{\beta t} & A_{\beta\beta} \end{bmatrix} \begin{Bmatrix} \ddot{q}_b \\ \ddot{q}_t \\ \ddot{\beta} \end{Bmatrix} + \rho V \begin{bmatrix} -\frac{cs}{10}a_w & 0 & 0 \\ -\frac{c^2 s}{8}b_w & \frac{-c^3 s}{24}M_{\dot{\theta}} & 0 \\ -\frac{c^2 s}{6}c_w & 0 & -\frac{-c^3 s}{8}M_{\dot{\beta}} \end{bmatrix} \begin{Bmatrix} \dot{q}_b \\ \dot{q}_t \\ \dot{\beta} \end{Bmatrix}$$
$$+(\rho V^2 \begin{bmatrix} 0 & \frac{cs}{8}a_w & \frac{cs}{6}a_c \\ 0 & -\frac{c^2 s}{6}b_w & -\frac{c^2 s}{4}b_c \\ 0 & -\frac{c^2 s}{4}c_w & -\frac{c^2 s}{2}c_c \end{bmatrix} + \begin{bmatrix} \frac{4EI}{s^3} & 0 & 0 \\ 0 & \frac{GJ}{s} & 0 \\ 0 & 0 & k_\beta \end{bmatrix}) \begin{Bmatrix} q_b \\ q_t \\ \beta \end{Bmatrix} = \begin{Bmatrix} 0 \\ 0 \\ 0 \end{Bmatrix} \tag{2}$$

which can also be written as its generalized form

$$\mathbf{A}\ddot{\mathbf{q}} + (\rho V \mathbf{B} + \mathbf{D})\dot{\mathbf{q}} + (\rho V^2 \mathbf{C} + \mathbf{E})\mathbf{q} = \mathbf{0} \tag{3}$$

Let **A** represent the inertia matrix, **B** denote the aerodynamic damping matrix, **D** symbolize the structural damping matrix, **C** denote the aerodynamic stiffness matrix, and **E** represent the structural stiffness matrix. $\ddot{\mathbf{q}}$, $\dot{\mathbf{q}}$ and **q**, are the acceleration, velocity, displacement vectors, respectively. Equation 2 assumes a symmetric inertia matrix, considering equal mass per unit of area for both the wing and control surface ($m_w = m_c = m$), with

$$A_{bb} = m\frac{sc}{5} \tag{4}$$
$$A_{tt} = m\frac{s}{3}(\frac{c^3}{3} - x_f c^2 + s_f^2 c) \tag{5}$$
$$A_{bt} = m\frac{s}{4}(\frac{c^2}{2} - x_f c) \tag{6}$$
$$A_{b\beta} = m\frac{s}{3}(\frac{c^2 - x_h^3}{2} - x_h(c - x_h)) \tag{7}$$
$$A_{t\beta} = m\frac{s}{2}(\frac{c^3 - x_h^3}{3} - (x_f + x_h)\frac{c^2 - x_h^2}{2} + x_f x_h(c - x_h)) \tag{8}$$
$$A_{\beta\beta} = ms(\frac{c^3 - x_h^3}{3} + x_h^2 c - x_h c^2) \tag{9}$$

For the aerodynamic damping (**B**) and stiffness(**C**) matrices, we have T_{10} T_{12} as Theodorsen functions (Theodorsen (1935)):

$$d = \frac{2x_h}{c} - 1 \tag{10}$$
$$T_{10} = \sqrt{1 - d^2} + cos^{-1} d \tag{11}$$
$$T_{12} = \sqrt{1 - d^2}(2 + d) + cos^{-1} d(2d + 1) \tag{12}$$

$a_w, b_w, c_w, a_c, c_c, d$ as being the lift, pitching and hinge moment coefficients, with Ec as the ratio of the control surface cord to the total cord

$$a_w = 2\pi \tag{13}$$
$$b_w = e a_w \tag{14}$$
$$c_w = -\frac{T_{12}}{2} \tag{15}$$
$$a_c = \frac{a_w}{\pi}[cos^{-1}(1 - 2Ec) + 2\sqrt{Ec(1 - Ec)}] \tag{16}$$
$$b_c = -\frac{a_w}{\pi}(1 - E)\sqrt{Ec(1 - Ec)} \tag{17}$$
$$c_c = -\frac{T_{12} T_{10}}{2\pi} \tag{18}$$

with $M_{\dot{\theta}}$ and $M_{\dot{\beta}}$ as being the non-dimensional pitch and control damping derivatives, respectively.

2.2 Eigenvalue Solution

For the solution of 2, or 3 to simplify, we use the eigenvalue solution by using the space-state representation to obtain the system natural frequencies and damping ratios at specifics flight conditions (Wright and Cooper (2015)). By combining the 3 with the trivial expression

$$\mathbf{I}\ddot{\mathbf{q}} - \mathbf{I}\dot{\mathbf{q}} = 0 \tag{19}$$

we obtain the now first order equation

$$\begin{Bmatrix}\dot{\mathbf{q}}\\ \ddot{\mathbf{q}}\end{Bmatrix} - \begin{bmatrix}0 & \mathbf{I}\\ -(\rho V^2\mathbf{C}+\mathbf{E}) & -\mathbf{A}^{-1}(\rho V\mathbf{B}+\mathbf{D})\end{bmatrix}\begin{Bmatrix}\mathbf{q}\\ \dot{\mathbf{q}}\end{Bmatrix} = \mathbf{0} \tag{20}$$

When assuming $\boldsymbol{q} = \boldsymbol{q_0}e^{\lambda t}$, the equation 21 can be obtained in its eigensolution form. The eigenvalues λ for an oscillatory system appear as complex conjugate pairs, as shown in equation 22 (Collar and Simpson (1987)).

$$[\lambda^2\boldsymbol{A} + \lambda(\rho V\boldsymbol{B}+\boldsymbol{D}) + (\rho V^2\boldsymbol{C}+\boldsymbol{E})]\boldsymbol{q_0} = \mathbf{0} \tag{21}$$

$$\lambda_j = -\zeta_j w_j \pm i w_j\sqrt{1-\zeta_j^2}, \quad j = 1,2,...,N \tag{22}$$

The stability of the aeroelastic system can be determined by analyzing the complex part of the eigenvalue. If it turns positive, then the system becomes unstable. We will employ the eigenvalue and eigenvector solution to solve the linear problem in the frequency domain. By doing so, we will determine the speed at which the system approaches flutter instability. This analysis will involve generating a graph of velocity-damping-frequency (v-g-f) to visualize the critical flutter speed and its corresponding damping and frequency values.

2.3 Fourth order Runge-Kutta Solution

The Runge-Kutta method involves obtaining an approximate solution to the Ordinary Differential Equation (ODE) at discrete points along an interval of interest. In contrast to the Euler method, which utilizes only a single estimate of the derivative, the Runge-Kutta method employs a weighted combination of several derivative estimates at different points within the interval (Iserles (2009)).

The central idea of the Runge-Kutta method is to divide the interval into several smaller sub intervals and calculate a weighted average of the derivatives within each sub interval. These weighted derivatives are then used to update the solution estimate at each discrete point. The method's accuracy can be adjusted by varying the number of points and the size of the sub intervals (Kim (2023)).

The fourth-order Runge-Kutta method, employed in this study, follows the same logic as the previous orders (Chapra and Canale (2015)). The most common form (Kim (2023)) is given by Equation 23 below:

$$y_{i+1} = y_i + \frac{1}{6}(k_1 + 2k_2 + 2k_3 + k_4)h \tag{23}$$

where

$$k_1 = f(x_i, y_i) \tag{24}$$
$$k_2 = f(x_i + \frac{1}{2}h, y_i + \frac{1}{2}k_1 h) \tag{25}$$
$$k_3 = f(x_i + \frac{1}{2}h, y_i + \frac{1}{2}k_2 h) \tag{26}$$
$$k_4 = f(x_i + h, y_i + k_3 h) \tag{27}$$

3. INCLUSION OF A NONLINEARITY

3.1 Hardening stiffness

The type of analysis to be used is known as bifurcation analysis. This type of analysis involves studying the nature of solutions as the system parameters vary. It explores qualitative changes in the solutions, such as variations in displacement,

as the parameters are modified. Bifurcation analysis is an important tool for understanding the complex dynamics of nonlinear systems and provides crucial insights into the stability and behavior of the system under different conditions (Bisplinghoff *et al.* (1996)).

In this study, It was added a cubic stiffness to our three-degree-of-freedom system (Bisplinghoff *et al.* (1996)). We will start by applying nonlinearity to the assumed translation mode stiffness k_z, which leads to a total stiffness of:

$$k_z z + k_{z3} z^3 \tag{28}$$

where k_{z3} is the cubic stiffness coefficient, which will be varied to obtain the results. The other parameters will remain the same as used in section 2.1 By applying the cubic stiffness to the equation obtained by state space expansion (20), which can be written as $\dot{\mathbf{x}} = \mathbf{Qx}$ where $\mathbf{Q}$ was obtained in section 2.2we have:

$$\dot{\mathbf{x}} = \mathbf{Qx} + \mathbf{L}k_{z3}\mathbf{z}^3 \tag{29}$$

where $\mathbf{L}$ is the matrix used to add non linearity, given by:

$$\mathbf{L} = \begin{bmatrix} -\mathbf{A}^{-1} \begin{bmatrix} 1 \\ 0 \\ 0 \end{bmatrix} \\ \mathbf{0}_{6x1} \end{bmatrix} \tag{30}$$

where the matrix $\mathbf{A}$ is the mass matrix defined in section 2.1The vector $\mathbf{z}$ is given by $\mathbf{z} = [z; 0; 0; 0; 0; 0; 0]$, where z is the vertical displacement.

It can be observed from Equation 30 that adding cubic stiffness affects all three degrees of freedom, showing a coupling of the system.

Similarly, the next bifurcation will be the addition of nonlinearity, this time in the stiffness of the torsional degree of freedom k_θ. This leads to a total stiffness of:

$$k_\theta \theta + k_{\theta 3} \theta^3 \tag{31}$$

where $k_{\theta 3}$ is the cubic stiffness coefficient, which will be varied to obtain the results. Similar to the previous non linearity, we have:

$$\dot{\mathbf{x}} = \mathbf{Qx} + \mathbf{M}k_{\theta 3}\theta^3 \tag{32}$$

where the matrix $\mathbf{M}$ is given by

$$\mathbf{M} = \begin{bmatrix} -\mathbf{A}^{-1} \begin{bmatrix} 0 \\ 1 \\ 0 \end{bmatrix} \\ \mathbf{0}_{6x1} \end{bmatrix} \tag{33}$$

and the cubic vector θ is given by $\theta = [0; \theta; 0; 0; 0; 0]$

Finally, an addition of cubic stiffness to the stiffness of the control surface rotation degree of freedom, resulting in a total stiffness of:

$$k_\beta \beta + k_{\beta 3} \beta^3 \tag{34}$$

where $k_{\beta 3}$ is the cubic stiffness coefficient. Analogously to the previous cases, we have:

$$\dot{\mathbf{x}} = \mathbf{Qx} + \mathbf{N}k_{\beta 3}\beta^3 \tag{35}$$

where $\mathbf{N}$ is given by

$$\mathbf{N} = \begin{bmatrix} -\mathbf{A}^{-1} \begin{bmatrix} 0 \\ 0 \\ 1 \end{bmatrix} \\ \mathbf{0}_{6x1} \end{bmatrix} \tag{36}$$

and the cubic vector β is $\beta = [0; 0; \beta; 0; 0; 0]$.

4. RESULTS

Drawing from the formulation presented in the preceding sections, numerical simulations were conducted to assess the impact of the nonlinearity on the aeroelastic system with three degrees of freedom. The parameters of the aeroelastic system, as given in Table 1, were employed alongside a Matlab® computer code that incorporates the procedures outlined in subsections 2.2 and 2.3.

Table 1. Data for the 3dof model wing with two degrees of freedom and a control surface

Parameter	Value	Parameter	Value
Semi-span (s)	7.5m	Torsional Rigidity (EI)	$4 \times 10^7 Nm^2$
Chord (c)	2m	Torsional Rigidity (GJ)	$8 \times 10^6\ Nm^2$
Position hinge line (x_h)	1.6m	Mass axis	1m
Position aerodynamic line (x_{ac})	0.5m	$M_{\dot{\theta}}$	-1.2
Position elastic axis (x_f)	0.8m	$M_{\dot{\beta}}$	-0.1
Distance from x_f to x_{ac}	0.3m	k_β	$1 \times 10^3 (Nm/m)/rad$

4.1 Analysis of the linear model in the frequency domain

As discussed in previous sections, there are various approaches to determine the flutter velocity of a dynamic aeroelastic system in the frequency domain. We can employ methods such as eigenvalue and eigenvector solutions, as well as the 'k' and 'p-k' methods. Once these methods are applied, we can generate a graph called the V-g-f diagram, which represents velocity on the horizontal axis, frequency on the upper vertical axis, and damping ratio on the lower vertical axis.

As mentioned in section 2.2, the analysis of eigenvalues and eigenvectors involves studying the coalescence of frequencies and the behavior of damping curves. The flutter speed is observed when the damping curve intersects the velocity axis, indicating the transition to positive damping. Furthermore, it is possible to determine the flutter speed by identifying the point at which the modal frequencies of the system converge or tend to converge to a common value.

Based on the data provided in Table 1, considering structural damping $\mathbf{D} = 0$, and using the model described in section 2. lwith the eigenvalue and eigenvector solution, it is possible to generate a v-g-f graph (Figure 2) using Matlab® software. Additionally, graphs were generated (Figure **??**) showing the frequencies of each mode, enabling the determination of the flutter critical speed for the aeroelastic problem of a two-degree-of-freedom model with a control surface.

The process to generate the V-g-f graph using Matlab® involves implementing the three-degree-of-freedom model in the software, solving the system of differential equations to obtain the corresponding eigenvalues and eigenvectors, and then plotting the results on the V-g-f graph. In accordance with the proposed data, it has been determined that the critical flutter velocity is $118m/s$.

Control frequency at 5.45 Hz and articulation point at 80% of the chord.

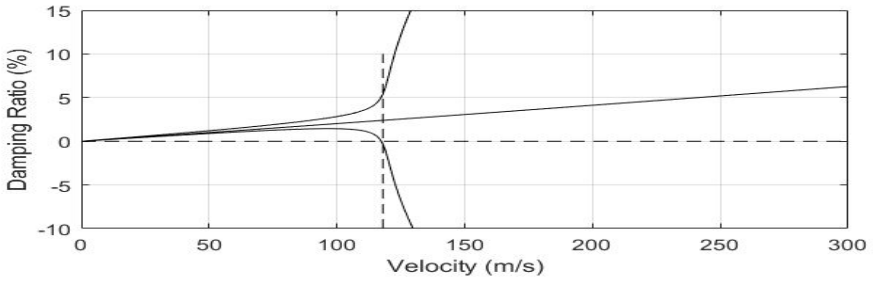

Figure 2. V-g-f graph

The utilization of the frequency domain solution allows for a more direct determination of the flutter critical velocity by observing the classic V-g-f diagram. Now, with the flutter critical velocity known, it is possible to examine the time-domain amplitude graphs at the flutter critical velocity. These time-domain graphs enable an analysis of how deformation evolves over time at different velocity regimes, clearly highlighting the differences before, during, and after flutter. This temporal analysis is crucial for understanding the dynamic behavior of the aeroelastic system and identifying potential instabilities or impacts on the structure.

5. COMPARISON BETWEEN LINEAR AND NONLINEAR MODELS

In this section, in order to enable a comparison between the two models, both the linear model, Equation 20, and the nonlinear model, as presented in Section 3, were numerically integrated over time using the fourth-order Runge-Kutta method, implemented through the 'ode45' function in Matlab® software. In this study, the torsional mode, θ, will be subjected to nonlinearity where an initial condition vector was set as $x_0 = [0.01, 0, 0, 0, 0, 0]$, and an integration time of [0, 15] seconds was considered for both the linear and nonlinear cases. In the nonlinear case, the equation presented in Section 3was integrated with a value for the cubic torsional nonlinearity of $k_{\theta 3} = 0.002k_\theta$. Thus, Figure 3 illustrates the time-domain amplitude of both the linear and nonlinear aeroelastic models at a flutter critical velocity of $V = 118m/s$.

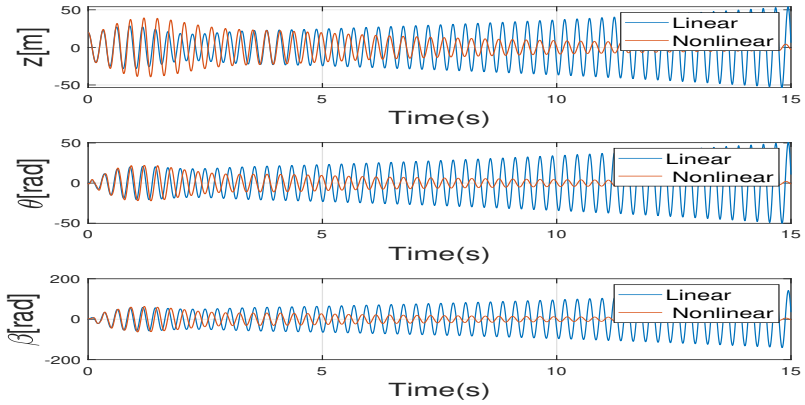

Figure 3. Time-displacement plot for linear and nonlinear models in the torsion mode (θ)

Figure 3 shows that in the linear case (blue line), oscillations grow exponentially, indicating flutter. In contrast, the nonlinear case (red line) exhibits a higher intensity initially due to the addition of nonlinearity, but it gets damped over time. It is observed that with the increase in the overall stiffness of the system, it becomes less susceptible to deformations and velocity increments, resulting in a damped response. The influence of increased stiffness on system stability is also evident, as oscillations decreased, in contrast to the linear case. It is also evident that the velocities exhibit a phase shift in the signal when comparing the linear and nonlinear models. It is possible to observe that the addition of nonlinearity in the torsional mode has a significant impact on the control surface torsional mode, demonstrating the mentioned coupling. This effect leads to a significant reduction in the amplitude of a potential Limit Cycle Oscillation (LCO).

Now, the cubic parameter will be varied while keeping the velocity fixed at the flutter critical velocity, $V = 118m/s$, to verify the influence of the nonlinearity. We will generate the graphs for $k_{\theta 3} = 0.0001k_\theta$ (Figure 4), $k_{\theta 3} = 0.001k_\theta$ (Figure 5), and $k_{\theta 3} = 0.0025k_\theta$ (Figure 6).

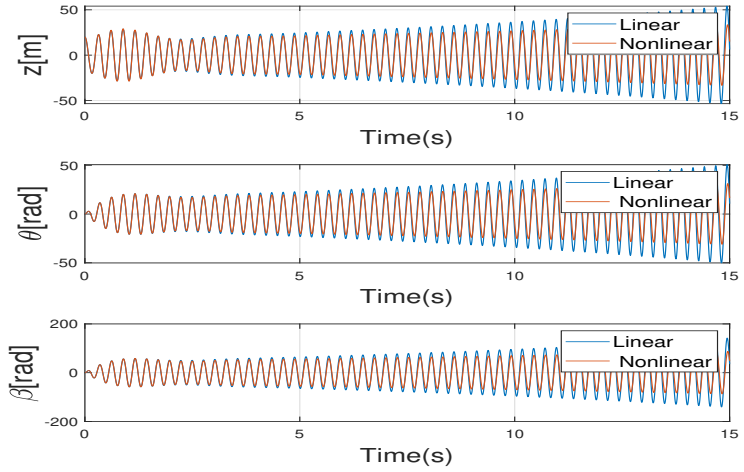

Figure 4. Time-displacement plot for linear and nonlinear models in the torsion mode (θ)

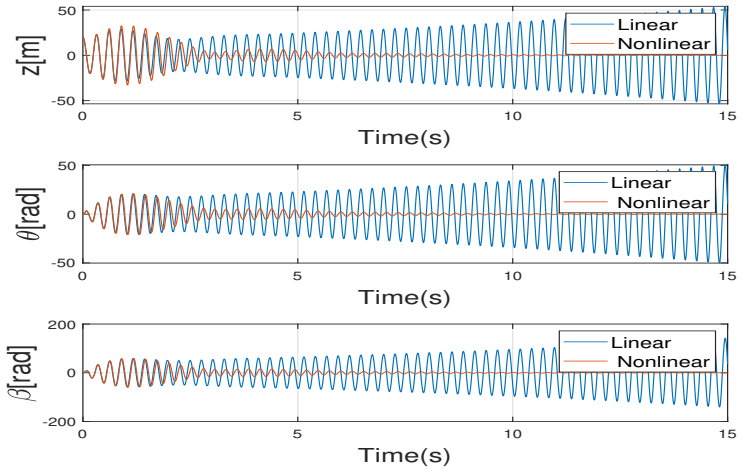

Figure 5. Time-displacement plot for linear and nonlinear models in the torsion mode (θ)

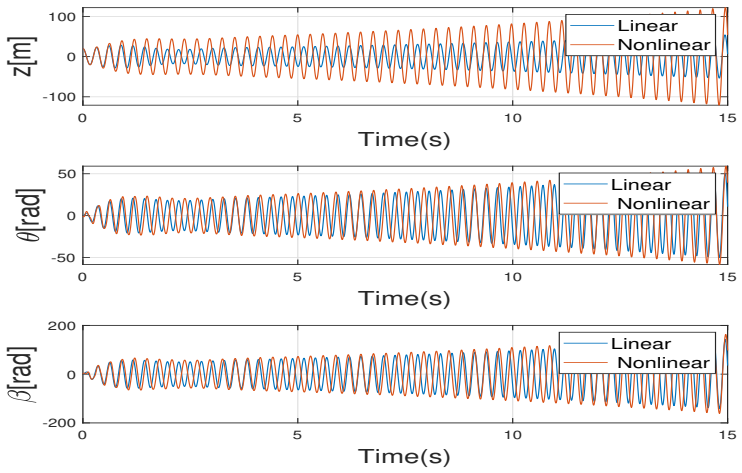

Figure 6. Time-displacement plot for linear and nonlinear models in the torsion mode (θ)

We can observe from Figures 5 and 4 that by reducing the cubic stiffness in the system, a decreasing oscillation occurs in the nonlinear model, but with a difference of phase between the models. With a further reduction, it is possible to observe that the amplitude in the nonlinear model resume its growth, but with no phase difference between the models, exhibiting a behavior similar to the linear model. This is consistent with the literature, which states that decreasing the value of the cubic nonlinearity coefficient brings the system closer to linearity (Dimitriadis (2017)).

On the other hand, with an increase in the coefficient of cubic stiffness (Figure 6), it is possible to observe oscillations of greater amplitude and more pronounced nonlinear behaviors, causing the nonlinear model to experience flutter more pronounced than the linear model. It is notable that even with the nonlinearity applied to θ, the oscillations exhibit greater amplitude and a greater phase lag between the models in β.

6. CONCLUSIONS

In this work, an aeroelastic stability analysis of a system was proposed with the inclusion of structural nonlinearities in the assumed torsional mode stiffness. The adopted model considers three degrees of freedom: two for the wing's bending and torsion and one for the control surface torsion. The nonlinearity was introduced through cubic stiffness. In the aerodynamic aspect, the model proposed by Hancock was utilized, which considers three-dimensionality of the flow using strip theory. The adopted aeroelastic model consists of a straight wing with three degrees of freedom, as proposed by Wright and Cooper. The aeroelastic equation for the system with three degrees of freedom was derived and used as the basis for the conducted analyses. The inclusion of structural nonlinearities was based on the models proposed by Dimitriadis. The cubic stiffness was introduced by multiplying the inverse of the mass matrix by a matrix of zeros, raising

the displacement terms of the degrees of freedom (z, θ, β) to the power of three. This nonlinearity was added in the torsion mode by adding a cubic term to the expanded aeroelastic state-space matrix to generate comparative graphs between linear and nonlinear models using Matlab®. V-g-f graphs were generated to determine the flutter velocity. Then, these velocities were used to generate graphs of velocity and displacement over time during critical velocity, both for linear and nonlinear models. We also analyzed the influence of nonlinearity by varying the coefficients of cubic stiffness and observed how these changes affected the nonlinear system. Comparing the two models after these analyses, we observed that the inclusion of nonlinearity affects each degree of freedom differently. While the linear model enters flutter, the nonlinear model is prevented from doing so with a cubic coefficient of 0.002 k_θ, also showing a difference of a phase between the models. We also found that reducing the nonlinearity coefficient to 0.001 k_θ leads to a reduction in the amplitude of the nonlinear model, but an even greater reduction, to a value of 0.0001 k_θ, shows an increase in the nonlinear model, but this time with no phase difference, approaching the nonlinear to the linear model, and that beyond a certain point, increasing the nonlinearity coefficient to 0.0025 k_θ causes the nonlinear model to enter flutter. As a continuation of this work, it is necessary to determine the critical velocity where the Limit Cycle Oscillation (LCO) can be observed more clearly. Moreover, obtaining a more accurate cubic coefficient is essential for a more practical analysis. This coefficient can be derived through either experimental analysis or numerical simulations.

7. ACKNOWLEDGEMENTS

The authors gratefully acknowledge the continued support to their work from CAPES, CNPq and Brasilia University.

8. REFERENCES

Bisplinghoff, R.L., Ashley, H. and Halfman, R.L., 1996. *Aeroelasticity*. Addison-Wesley Publishing Company, Inc. ISBN 978-0486691893.

Chapra, S.C. and Canale, R.P., 2015. *Numerical Methods for Engineers*. McGraw-Hill Education. ISBN 978–0–07–339792–4.

Collar, A.R. and Simpson, A., 1987. *Matrices and Engineering Dynamics*. John Wiley Sons Inc. ISBN 978-0470202715.

Dimitriadis, G., 2017. *Introduction to Nonlinear Aeroleasticity*. John Wiley Sons Ltd. ISBN 9781118756454.

Iserles, A., 2009. *A First Course in the Numerical Analysis of Differential Equations*. Cambridge University Press. ISBN 978-0-511-50637-6.

Kim, S., 2023. *Numerical Methods for Partial Differential Equations*. Department of Mathematics and Statistics Mississippi State University. ISBN 978–0–07–339792–4.

Theodorsen, T., 1935. *General Theory of Aerodynamic Instability and the Mechanism of Flutter*. National Advisory Commitee for Aeronautics NACA report 496, AERADE Reports Archive.

Wright, J.R. and Cooper, J.E., 2015. *Introduction to Aircraft Aeroelasticity and Loads*. John Wiley & Sons. ISBN 978-1-118-48801-0.

9. RESPONSIBILITY NOTICE

The authors are solely responsible for the printed material included in this paper.